Analysis of Electromagnetic Scattering Using Arrays of Fictitious Sources

Yehuda Leviatan, *Senior Member, IEEE*, Zachi Baharav, *Student Member, IEEE*, and Ehud Heyman, *Senior Member, IEEE*

Abstract— **The use of models of fictitious elemental current sources, located inside the scatterer to simulate the scattered field, has proved to be an efficient computational technique for analyzing scattering by metallic bodies. This paper presents a novel modification of the technique in which the omnidirectional elemental sources are arranged in groups of array sources with directional radiation patterns, and the boundary testing points are arranged in groups of testing arrays with directional receiving patterns. This modification which is motivated by physical understanding is equivalent to mathematical basis transformations. It renders the system matrix more localized and thereby enables the analysis of larger bodies. The new approach is applied to the case of TM scattering by a perfectly conducting square cylinder with side-length of 20λ. Reduction of 50% in the number of the nonzero elements of the system matrix is achieved with virtually no degradation in the accuracy of the radar cross section (RCS) calculations.**

radiate directional beams. Likewise, the set of boundary testing points which individually are isotropic receptors is divided into groups to form testing arrays with directional receiving patterns. This process can be equivalently effected, however, by simply applying appropriate basis transformations to the original matrix equation obtained, based on a conventional current-model solution.

The paper is organized as follows. In Section II, the fictitious source formulation is briefly outlined and notations are established. Section III, which constitutes the main body of the paper, is devoted to the presentation of general bases-transformations from both the physical and mathematical points of view. In Sections IV and V, two useful transformations are described. Section VI contains the results of an application of the approach for a large square cylinder. In

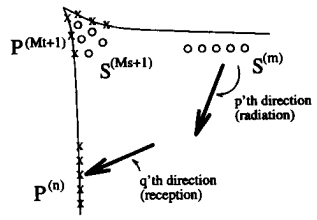

Fig. 1. The fictitious array approach. The fictitious sources near the smooth parts of the scatterer (circles) are arranged in M_s groups of array sources $\{S^{(m)}\}_{m=1}^{M_s}$. The sources near the rapidly varying parts of the boundary are considered individually, and we refer to this group of sources as the (M_s+1)th group. The testing points (crosses) are arranged in a similar way. Those on the smooth parts of the boundary are arranged in M_t groups of testing arrays $\{P^{(n)}\}_{n=1}^{M_t}$, while the ones on the rapidly varying parts of the boundary are considered individually, and we refer to this latter group as the (M_t+1)th group. The vector of unknown source amplitudes, $\vec{I}^{(m)}$, is then derived from a vector of unknown array amplitudes $\vec{A}^{(m)}$ through a linear transformation $[T]^{(m)}$ representing the amplitudes of the mth array when radiating in different spatial directions. Likewise, the known vector of source excitations, $\vec{V}^{(n)}$, is transformed to a vector of array excitations $\vec{B}^{(n)}$ via a linear transformation $[Q]^{(n)}$. The significant elements of the modified impedance matrix $[Z]$ would be only those corresponding to strong coupling between the array sources and the matching arrays. Strong coupling would occur when the direction of an array source main beam coincides with a direction of maximum reception of a testing array.

where $\vec{I}$ is an N_s-element vector of the unknown amplitudes, $\vec{V}$ is an N_t-element excitation vector whose mth element is $-E_z^{\text{inc}}(\boldsymbol{t}_m)$, and $[Z]$ is an $N_t \times N_s$ system (or impedance) matrix whose mnth element is $G(\boldsymbol{t}_m, \boldsymbol{r}_n)$. Namely, the mnth element of $[Z]$ is the field at testing point $\boldsymbol{t}_m$ due to a unit-amplitude source centered at $\boldsymbol{r}_n$.

III. Basis Transformations

In this section, the transformation which modifies the conventional system matrix $[Z]$ to the one corresponding to the directional array sources and directional testing arrays is described. Specific examples will follow in the sequel.

Throughout the following, two concepts are intertwined. One is the physical point of view which stimulated the idea of transforming the omnidirectional sources into directional array sources. The other is the idea of basis transformation via matrix multiplications which facilitates the necessary mathematical tools.

Let us divide the set of source points $\{\boldsymbol{r}_i^s\}$ into groups of $\{S^{(m)}\}_{m=1}^{M_s+1}$, each composed of the elements $\{\vec{I}_i^{(m)}\}_{i=1}^{N^{(m)}}$. Each of the first M_s groups is treated as an array source. In the (M_s+1)th group, the sources are considered individually. As a general practice, the first M_s groups are located near and associated with the smooth parts of the scatterer, while the (M_s+1) group is composed of the sources located near and associated with the irregular parts of the scatterer such as corners and sharp edges (see Fig. 1).

We now explore a transformation $[T]^{(m)}$ that associates with the vector $\vec{I}^{(m)}$, composed of $N^{(m)}$ independent amplitudes of omnidirectional sources, a vector $\vec{A}^{(m)}$, composed of $N_A^{(m)}(\leq N^{(m)})$ independent amplitudes of directional array sources. Each array source is formed by a combination of omnidirectional sources and corresponds to a specific excitation of these omnidirectional sources. Towards this end, we construct a matrix $[T]^{(m)}$ in which the pth column consists of the amplitudes of the single sources used to form a unit-amplitude array source ($A_p^{(m)} = 1$). Thus, we have

$$\vec{I}^{(m)} = [T]^{(m)}\vec{A}^{(m)}. \tag{3}$$

Combining the transformations associated with the various groups into one source-transformation matrix $[T]$, satisfying $\vec{I} = [T]\vec{A}$, we obtain

$$[T] = \begin{pmatrix} [T]^{(1)} & & \\ & \ddots & \\ & & [T]^{(M_s)} \\ & & & [I_{N^{(M_s+1)}}] \end{pmatrix} \tag{4}$$

where $[I_{N^{(M_s+1)}}]$ is the square identity matrix of size $N^{(M_s+1)}$. This identity matrix is due to the fact that the $S^{(M_s+1)}$ group remains unchanged.

Thus, (2) can be written as

$$\vec{V} = [Z]\vec{I} = [Z][T]\vec{A} = [Z_A]\vec{A} \tag{5}$$

where

$$[Z_A] \triangleq [Z][T]. \tag{6}$$

It is important to draw attention again to the physical interpretation of the transformation. $[Z_A]$ is composed of M_s+1 groups of columns. The mth group of columns is the result of multiplying the corresponding columns of $[Z]$ with $[T]^{(m)}$. Thus, the (q,p) element in this group represents the field at the qth testing point due to a unit amplitude excitation of the pth array source in the mth set of array sources ($A_p^{(m)} = 1$). Since this array source is a directional one, we expect that for testing points that fall within the main lobe of its radiation pattern, the value of the corresponding elements in the matrix will be relatively large. On the other hand, for testing points that do not fall within its main lobe, this value will be relatively small.

Similar operations can be practiced with the testing points. Accordingly, the testing points are divided into M_t+1 groups, $\{P^{(n)}\}_{n=1}^{M_t+1}$, and transformations $[Q]^{(n)}$ are introduced that associate with the excitation vector $\vec{V}^{(n)}$, a vector $\vec{B}^{(n)}$ composed of the weighted excitations of the testing array. We have

$$[Q]^{(n)}\vec{V}^{(n)} = \vec{B}^{(n)}. \tag{7}$$

The structure of $[Q]^{(n)}$ can be explained as follows: The qth row of $[Q]^{(n)}$ is the weighting of the individual testing points, equivalent to a unit weighting of the testing array $B_q^{(n)}$.

Combining the transformations associated with the various groups into one testing-transformation matrix $[Q]$, satisfying $[Q]\vec{V} = \vec{B}$, we obtain

$$[Q] = \begin{pmatrix} [Q]^{(1)} & & \\ & \ddots & \\ & & [Q]^{(M_t)} \\ & & & [I_{N^{(M_t+1)}}] \end{pmatrix} \tag{8}$$

where the notations follow the previously described ones.

Thus, (2) reduces to

$$[Q]\vec{V} = \vec{B} = [Q][Z][T]\vec{A} = [\mathcal{Z}][A] \tag{9}$$

where

$$[\mathcal{Z}] \triangleq [Q][Z][T]. \tag{10}$$

As described earlier, the magnitude spread of the elements of the new matrix $[\mathcal{Z}]$ will be less uniform than that of $[Z]$. That is, only a few elements will be of large values (array source and testing array direction coincidence), while most of the other elements will be extremely small (direction mismatch).

Since $[T]$ and $[Q]$ are block-diagonal, the matrix $[\mathcal{Z}]$ consists of $(M_t + 1) \times (M_s + 1)$ blocks $[\mathcal{Z}]^{(n,m)}$ given by

$$[\mathcal{Z}]^{(n,m)} = [Q]^{(n)}[Z]^{(n,m)}[T]^{(m)} \tag{11}$$

where $[Z]^{(n,m)}$ is the block in the original matrix $[Z]$, corresponding to the nth testing array and the mth array source. For physical interpretation, we shall express the (q,p) element in $[\mathcal{Z}]^{(n,m)}$ explicitly as

$$[\mathcal{Z}]^{(n,m)}_{q,p} = \sum_{l=1}^{N^{(m)}} \sum_{i=1}^{N^{(n)}} [Q]^{(n)}_{qi}[Z]^{(n,m)}_{il}[T]^{(m)}_{lp}. \tag{12}$$

The physical interpretation of $[\mathcal{Z}]^{(n,m)}_{q,p}$ is as follows: it describes the field produced by the pth set of excitations of the mth array source (the pth column in $[T]^{(m)}$) at any point i of the nth testing array, weighted by the qth set of weighting (qth row of $[Q]^{(n)}$). Consequently, it is anticipated that $[\mathcal{Z}]^{(n,m)}_{q,p}$ will be significant only if both the pth set of array excitation of $\{S\}^{(m)}$ will enhance radiation toward $\{P\}^{(n)}$ and if the qth set of weighting of the test array $\{P\}^{(n)}$ will be matched for radiation from the direction of $\{S\}^{(m)}$ (see Fig. 1).

It should be mentioned that the last column of blocks (the $(M_s + 1)$th) in $[\mathcal{Z}]$ is given by

$$[\mathcal{Z}]^{(n,M_s+1)} = [Q]^{(n)}[Z]^{(n,M_s+1)} \tag{13}$$

and describes the radiation by point sources that are located near the edges and are not treated collectively as arrays. Similarly, the last row of blocks (the $(M_t + 1)$th) is given by

$$[\mathcal{Z}]^{(M_t+1,m)} = [Z]^{(M_t+1,m)}[T]^{(m)} \tag{14}$$

and accounts for reception by individual test points that are located near the edges. Note also that

$$[\mathcal{Z}]^{(M_t+1,M_s+1)} = [Z]^{(M_t+1,M_s+1)}. \tag{15}$$

In the following sections, two transformations will be introduced. Before proceeding further, however, the following aspects which can aid when comparing between these transformations should be noted.

- *Sparseness of matrix versus thresholding value*—Thresholding is the (nonlinear) process of equating to zero all the matrix elements with magnitude below a specified threshold. This process produces a sparse matrix. The matrix sparseness is defined as the ratio of the number of zero-elements in the matrix and the total number of elements. To eliminate the influence of a constant multiplier, the threshold is performed on a "normalized" matrix, a matrix in which the largest element is of unit magnitude. We anticipate that for any given threshold, the transformed matrix will be sparser due to the fact that its elements are less uniformly distributed. This, in turn, is due to the directivity of the sources which strongly effect the interaction between sources and test points.
- *Sparseness of matrix versus solution accuracy*—By specifying a magnitude threshold and setting to zero all the elements of $[\mathcal{Z}]$ that fall below this level, a sparse matrix is obtained. The solution accuracy, however, may be strongly affected by this nonlinear operation. The solution should therefore be compared to the exact one under the criterion of interest, be it the near-field, far-field, or any other quantity.
- *Computational complexity*—The transformations described require extra computations above those needed for computing $[Z]$. This is expected to be compensated for, however, by the advantages gained from the sparseness of the matrix.
- *Condition number of* $[\mathcal{Z}]$—The condition number gives an estimate of how small an element should be so that it might be set to zero without significantly affecting the result. It also serves as a good estimate to the solution (of the matrix inversion problem) convergence rate. As will be seen shortly, however, the transformations used are unitary, and thus the condition number of $[Z]$ is not altered by the transformations. Moreover, the condition number of $[Z]$ strongly depends on parameters associated with the fictitious-sources method (i.e., distance between the sources and the surface, the spacing between sources). Thus, we will not discuss the condition number in detail because it is much more a characteristic of the underlying fictitious source model method rather than a feature of the transformations.

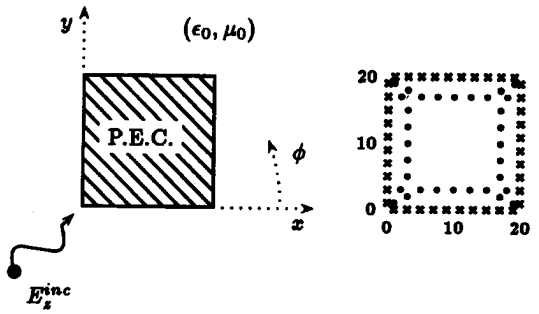

Fig. 2. (a) Problem definition. (b) Schematic location of source points ("o") and testing points ("×") (see details in text). The numbers on the axes are in units of wavelength.

It should be clear that in all cases the effectiveness of the transformation is inherently related to the geometry of the problem. Thus, the results which follow may only be indicative for other configurations and transformations. Here we consider the case of the scattering of a plane-wave by a perfectly-conducting square cylinder with side length of 20λ. The geometry of the problem together with a schematic

representation of the location of the sources and testing points is shown in Fig. 2. A source-model solution of this kind has already been applied to a similar problem in [6]. The sources are located as follows: There are four side segments, each retracted by 0.3λ from the corresponding side of the body. Considerations as to the proper choice of source locations can be found in [7]. Each side segment consists of 84 equispaced sources and extends 18λ in length. In addition, there are eight corner segments, each comprising ten equispaced sources, extending from the corners to a point $(1\lambda, 0.3\lambda)$ interior to the body. The testing points are located on the cylinder perimeter. There is a total of 208 testing points per side (twice the number of source points).

IV. DFT Transformation (Linear Arrays)

Perhaps the simplest and most direct way to transform the source amplitude-vector $\vec{I}^{(m)}$ to the array amplitude vector $\vec{A}^{(m)}$ is by the use of the discrete Fourier transform (DFT). Following (3), while assuming $N^{(m)}$ (the number of elements in the group $S^{(m)}$) is odd, the elements of $\vec{I}^{(m)}$ and $\vec{A}^{(m)}$ are related via

$$I_l^{(m)} = \sum_{p=-(N^{(m)}-1)/2}^{(N^{(m)}-1)/2} W_{lp}^{(m)} A_p^{(m)} \tag{16}$$

where

$$W_{lp}^{(m)} = \frac{1}{\sqrt{N^{(m)}}} \exp\left(j \frac{2\pi}{N^{(m)}} lp\right). \tag{17}$$

Writing (16) in a matrix form, yields

$$\vec{I}^{(m)} = [W]^{(m)} \vec{A}^{(m)} \tag{18}$$

where $[W]^{(m)}$ is the DFT matrix, defined by (17). Note that to facilitate a simple physical interpretation of the transformation, the indexes we use are in the symmetric interval $[-(N^{(m)} - 1)/2, (N^{(m)} - 1)/2]$. Equation (18) is a special case of (3) with $[T]^{(m)} \rightarrow [W]^{(m)}$. This choice suggests the following interpretation for the coefficients $A_p^{(m)}$. If the source points in the m group are colinear and equispaced, then the new variables $\{A_p^{(m)}\}$ represent coefficients of linear arrays. Each array of this kind is composed of identical sources, all with the same amplitude and each with a progressive phase of $((2\pi/N^{(m)})lp)$. Thus, $A_p^{(m)}$ correspond to a linearly phased array whose radiation angle with respect to the broadside direction satisfies

$$\sin(\varphi_p^{(m)}) = \frac{\lambda}{N^{(m)} d^{(m)}} p = \frac{\lambda}{D^{(m)}} p. \tag{19}$$

Here, $D^{(m)}$ denotes the total length of the mth array, and $d^{(m)}$ denotes the distance between the array elements. Note that for positive value of p, the array main beam is on the right-hand side of broadside, whereas for negative values of p it is on the left-hand side of broadside. Note that only terms with

$$|p| < \frac{D^{(m)}}{\lambda} \tag{20}$$

correspond to propagating beams. For $|p| > D^{(m)}/\lambda$, the phase gradient between the elements is larger than the wavenumber k, and the array generates an evanescent field which is localized in the near vicinity of the array. Thus, the mth group is essentially comprised of

$$p_0 = 2\left\lfloor \frac{D^{(m)}}{\lambda} \right\rfloor + 1 \tag{21}$$

arrays that emanate propagating beams. Often, the elements are arranged in sizable groups. Hence $D^{(m)} \gg \lambda$, and there is a large number of propagating beams. All the other arrays generate eventually evanescent fields. The largest wavenumber along the array, $k_{t_{\max}}$, is given by

$$k_{t_{\max}} = \frac{2\pi}{d^{(m)}} \frac{1}{2} \frac{N^{(m)} - 1}{N^{(m)}} \approx \frac{1}{2} \frac{2\pi}{d^{(m)}} \tag{22}$$

where the approximate expression applies, provided that $N^{(m)} \gg 1$. Note that near the smooth section of the boundary one may choose to increase the distance $d^{(m)}$ between the elements. In view of (21), this will not reduce the sampling rate of the real spectrum, but (22) implies that this will limit the maximum wavenumber described by the source distribution. For example, $k_{t_{\max}} \approx 2k$ yields $d^{(m)} \approx \lambda/4$.

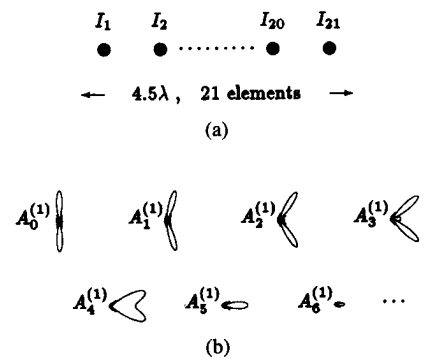

Fig. 3. (a) Original set of omnidirectional sources which are transformed via $[T]_{21\times21}$: $\{T_{mn}\} = \exp(j(2\pi/21) \cdot m \cdot n)$ to a set of directional linear array sources. (b) Radiation patterns of the array sources (all patterns are far-field patterns).

Fig. 3 gives a pictorial illustration of how the transformation works. Fig. 3(a) shows a set of $N^{(m)} = 21$ single sources which are taken to form a group. We assume, for future purposes, that the sources are equispaced and colinear. Using $[T]_{21\times21}$: $\{T_{mn}\} = \exp(j(2\pi/21) \cdot m \cdot n)$, the original set of omnidirectional sources is transformed to a set of directional linear array sources. Hence, instead of using the 21 independent amplitudes of the omnidirectional sources, we deal now with 21 new, independent amplitudes which relate to directional arrays. The far-field radiation patterns of the array sources are depicted in Fig. 3(b). From (20), it follows that there is a total of nine propagating beams and 12 evanescent fields. Shown are the broad-side pattern and the patterns on its right-hand side. The patterns on the left-hand side of broadside (not shown) are, of course, symmetrical to those on the right-hand side. Here, the broadside pattern and the first four patterns on its right correspond to propagating beams. The other patterns shown correspond to evanescent fields. It should be clear that in this figure's configuration, any radiation pattern attainable by the 21 independent sources is

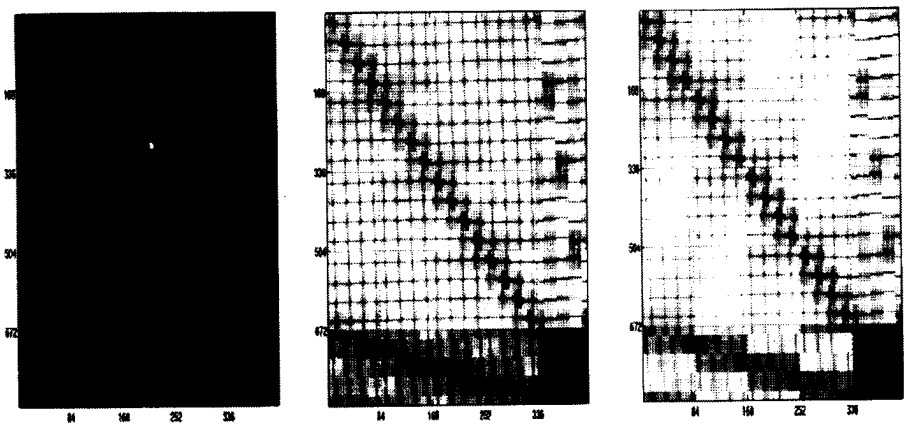

(a) (b) (c)

Fig. 4. Structure of the impedance matrix (elements of higher magnitude are shown darker) for the cases: (a) single sources (no transformation), (b) linear array sources, and (c) double-layer array sources. Marked on the horizontal and vertical axes are the matrix row and column numbers, respectively.

also achievable by the 21 array sources, and vice-versa, which is also evident from the fact that $[T]^{(m)}$ is invertible.

In a similar manner, the same transformation is applied to the testing points. We denote this transformation by $[\tilde{W}]^{(n)}$. The tilde is used to indicate that this transformation may be different from $[W]^{(n)}$ as there may be more testing points than sources. Thus, we let

$$[\tilde{W}]^{(n)}\vec{V}^{(n)} = \vec{B}^{(n)} \tag{23}$$

and readily obtain the new impedance matrix

$$[\mathcal{Z}] = [\tilde{W}][Z][W]. \tag{24}$$

The grouping of the source/testing points in the specific scattering problem we consider is as follows: Each of the side segments is divided into four groups of sources, each comprising 21 sources. The sources in the eight corner segments are combined into one group which is left unchanged by the transformation. The testing points are grouped in a similar manner. The structure of $[Z]$ and $[\mathcal{Z}]$ is shown in Fig. 4(a) and (b), respectively. In both cases, dotted lines were drawn to mark the different five regions: the first four describe the interaction between the four side segments of the square (each containing four array sources), and the fifth region describes interaction involving the single elements near the corners. In Fig. 4(a), the structure of the conventional (i.e., before transformation) impedance matrix is shown. The only parameter determining magnitude of the elements is the distance between the source point and the testing point. Thus, the elements on the diagonal are large in magnitude, and this element magnitude falls as one recedes from the diagonal. The effect of the array directivity is readily observed in Fig. 4(b), especially in the part of the matrix corresponding to the intersection of the first four blocks of columns and rows. This region describes the interaction of array sources and test arrays. If the main lobes of the receiving and radiation patterns do not coincide, the corresponding diagonal elements are small even when the source array and testing array are close. Also, clearly seen is the partition of each side to four arrays. The curvature of the pattern of dark lines in the matrix stems from the dynamics of the array source and testing array coupling. A smaller degree of sparseness is exhibited by the fifth block of columns and the fifth block of rows: they describe, respectively, the interactions of the array sources along the sides with the individual testing points near the corners and the interactions of the individual point sources near the corners with the testing arrays along the sides, and are given, respectively, in (13) and (15).

V. Double-Layer Arrays

This section takes the previously discussed ideas one step further. As noted earlier, the radiation field produced by the linear array sources is directed not only towards the nearby boundary in front of them, but also backwards towards the interior of the object. Hence, when the direction of the array-source main beam coincides with the maximum direction-of-reception of the testing array, the corresponding elements in the matrix $\mathcal{Z}$ may be quite significant (see Fig. 1 for an illustrated description of such a coupling).

A sparser matrix could therefore be achieved if the sources are arranged so that they can be grouped into new kinds of arrays which radiate only in the forward direction. An array that has this desired property can be constructed by adding to each linear array an identical parallel array which is retracted a distance h towards the interior of the body. The amplitudes of respective elements in the two arrays are not independent. The amplitudes of the rear elements are the same as those of the front ones except for a $\psi = e^{jkh}$ phase lead. With a proper choice of h, the radiation of the double-layer array towards the interior of the body can be strongly suppressed. For example, the choice of $h = \lambda/4$ and a corresponding phase lead of $\psi = \pi/2$ would yield a null in the backward broad-side direction. A double-layer array with $h = \lambda/4$ and $\psi = \pi/2$ is depicted in Fig. 5. A similar idea of constructing directional sources via the combination of electric and magnetic currents can be found in [8].

To construct double-layer arrays for the square-cylinder scattering problem, one can start with the previously described configuration of sources and then add to the side segments a parallel set of sources retracted by $\lambda/4$ towards the interior of the body. Next, we construct the conventional impedance ma-

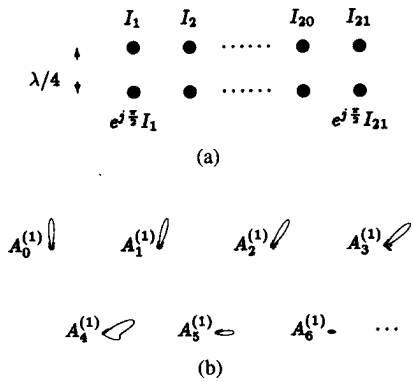

Fig. 5. Double-layer array: (a) Element locations and amplitude relations and (b) Radiation patterns, analogous to those shown in Fig. 3(b) for the single-layer arrays.

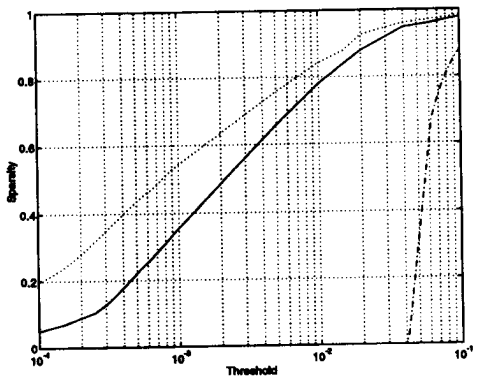

Fig. 6. Sparseness of impedance matrix as a function of threshold value for the three cases: (a) Single sources (nontransformation) (dash-dot line), (b) Four array sources per side (DFT transformation) (solid line), and (c) Double-layer array (dotted line).

trices, say $[Z]^{(n,m)}$, for the interaction between the individual elements comprising the mth double-layer array source and the individual testing points comprising the nth testing array as though they were all independent sources. Then, we use the transformation matrix

$$[T]^{(m)} = \begin{bmatrix} [W]^{(m)} \\ e^{j(\pi/2)} \cdot [W]^{(m)} \end{bmatrix} \tag{25}$$

to transform the sources amplitude vector $\vec{I}^{(m)}$ to the (double-layer) array amplitudes $\vec{A}^{(m)}$ via (18). Similarly, we use $[Q]^{(n)} = [\tilde{W}]^{(n)}$ to transform $\vec{V}^{(n)}$ into the testing array vector $\vec{B}^{(n)}$ via (23). Finally, we evaluate $[\mathcal{Z}]$ using (10).

The structure of the resulting impedance matrix $[\mathcal{Z}]$ is shown in Fig. 4(c). Comparing Fig. 4(c) with (b), one observes that the directivity of the arrays almost totally eliminates the interaction between the array on one side of the cylinder and the testing points on the opposite side.

VI. Simulation Results and Discussion

In this section we turn to investigate the two transformations (DFT and double-layer) according to the previously described aspects and compare them with the regular (nontransformation) case. This is done on the previously described configuration of TM scattering by a large, square cylinder.

- *Matrix sparseness versus threshold value*—In Fig. 6 the sparseness of the impedance matrices is described as a function of the threshold. From the figure it is clear that for a given threshold, the transformed matrices are much sparser than the original one (note that the scale is logarithmic).
- *Sparseness of matrix versus accuracy of solution*—Fig. 7(a) describes the scattering width obtained based on the conventional source-model solution without any thresholding. The results have been compared with a reference solution [9] (not shown), which is based on the generalized multipole technique [10], [11]. The agreement between our result and the result of the reference solution is impeccable. Fig. 7(b) shows results for the scattering width and exemplifies how even a slight thresholding of the impedance matrix affects the accuracy. Next, Fig. 8(a) describes the scattering width obtained using linear arrays (DFT transformation) and a subsequent thresholding operation which leaves 87% of the matrix elements unaffected while setting the remaining elements equal to zero. Note that the accuracy achieved with this reduced number of matrix elements is excellent. This accuracy remains quite reasonable even when the thresholding operation is carried further to yield a fractional number of nonzero matrix elements of approximately two-thirds. In this latter case, shown in Fig. 8(b), the deviation from the accurate solution becomes noticeable. Finally, Fig. 9(a) describes the scattering width obtained using double-layer arrays and a subsequent thresholding operation which leaves 51.6% of the matrix elements unaffected while setting the remaining elements equal to zero. Note that the accuracy achieved with this reduction to nearly half the number of matrix elements is remarkable. This accuracy remains quite reasonable even when the fractional number of nonzero matrix elements is further reduced up to approximately one-third. In this latter case, shown in Fig. 9(b), the deviation from the accurate solution again becomes noticeable. Clearly, the use of the proposed transformations enables one to substantially reduce the number of significant elements in the impedance matrix. It is also interesting to mention that, as expected, the dominant elements in the solution (i.e., the p and m for which $A_p^{(m)}$ is the largest) correspond to arrays radiating in the anticipated directions predicated by geometrical optics.
- *Computational complexity*—In the case of the DFT based transformations, one can resort to existing effective techniques for fast computation of the transform (FFT). The sparseness of the matrix enables us to use the special functions in Matlab-4.2 that deal exclusively with sparse matrices. These functions exploit the fact that for a sparse matrix both a smaller storage space is needed and fast multiplication algorithms exist. They do not, however, take advantage of the special banded structure characterizing the previously described matrices.

VII. Comparison with Related Methods

An idea very similar to that advocated here has been

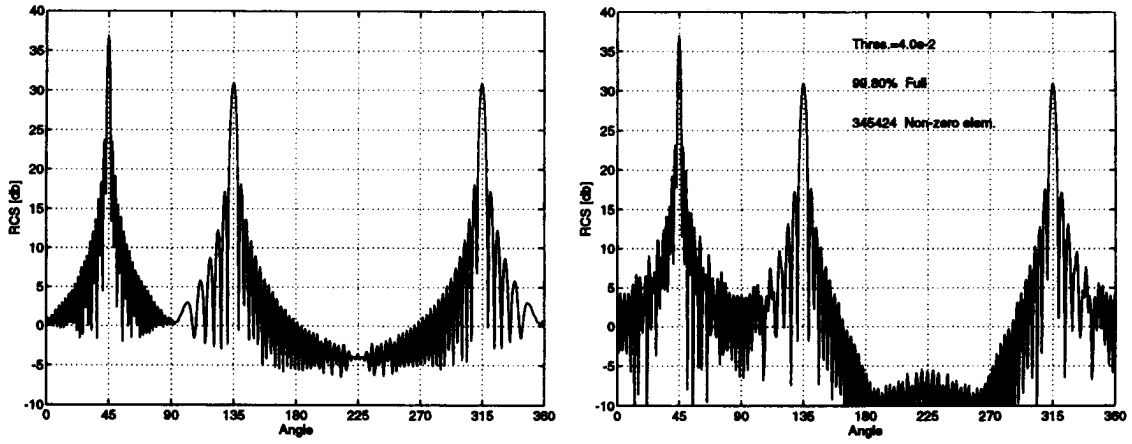

(a) (b)

Fig. 7. Bistatic scattering width obtained based on the conventional source-model solution (a) with no thresholding and (b) with a relatively slight reduction in the number of matrix elements.

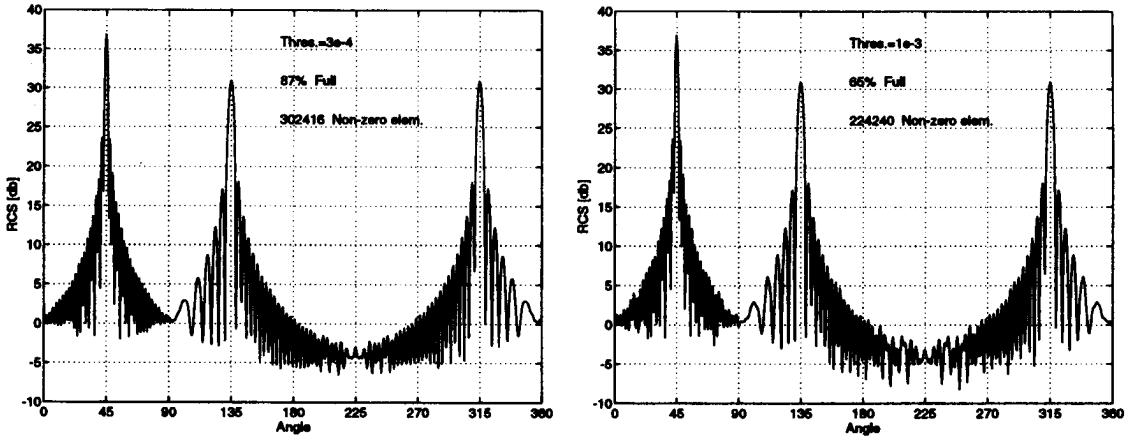

(a) (b)

Fig. 8. Bistatic scattering width obtained using linear array sources and thresholding operations which leave (a) 87% and (b) 65% of the matrix elements unaffected while setting the remaining elements equal to zero.

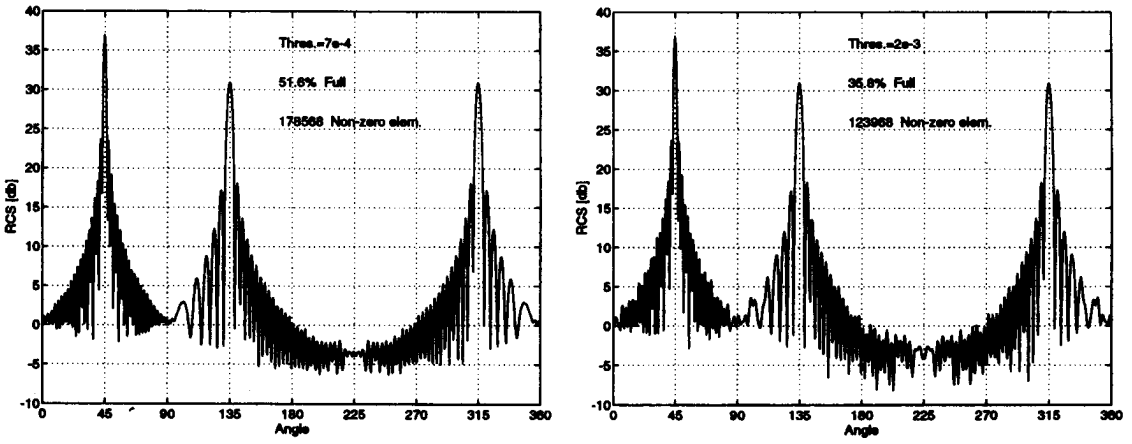

(a) (b)

Fig. 9. Bistatic scattering width obtained using double-layer array sources and thresholding which leaves (a) 51.6% and (b) 35.8% of the matrix elements unaffected while setting the remaining elements equal to zero.

utilized in the impedance matrix localization (IML) method, suggested by Canning [2]–[5]. Others have also suggested the use of directional fictitious sources [12], [13]. In the IML method, the starting point is a method of moments (MoM) formulation of the problem using pulse-basis functions. A transformation which yields piecewise constant functions

smoother than pulses is then applied to the sources and hence to the impedance matrix. Compared with Canning's solution, the present approach has two merits. The first attractive feature is related to the basic advantage of the source-model technique over the standard MoM. It lies in the more appropriate approximation of the unknown surface current by means of smooth rather than by piecewise constant expansion functions. The other merit is the simplicity and versatility afforded in synthesizing new array sources for the fields and similarly new receiving arrays for testing, both with directional patterns designed as per requirement.

VIII. Summary and Conclusions

The use of models of fictitious sources has been known as a technique for solving scattering problems for quite some time. By using a basis transformation based on physical insight (directivity of sources), a more sparse representation of the impedance matrix was readily achieved. This was further improved by applying a similar idea to the testing points. Two different transformations have been described, each yielding a sparse matrix without a considerable loss in the solution accuracy. As mentioned in the text, the transformation is related to the geometry of the problem. Another case of interest is that of concave bodies. In this case, arrays located along the inwardly curved parts of the body will face one another and have strong interaction between them. Hence, the resultant impedance matrix will generally be less localized. To achieve higher localization in this case, one can resort to a design of arrays other than linear ones. Thus, future directions may include the examination of other array patterns tailored to match specific problems. Moreover, even for a given geometry and a given sources locations, it is still an open question which of the array modes should be preferred. These ideas are currently under investigation.

References

[1] Y. Leviatan, A. Boag, and A. Boag, "Generalized formulations for electromagnetic scattering from perfectly conducting and homogeneous material bodies-theory and numerical solution," *IEEE Trans. Antennas Propagat.*, vol. 36, no. 12, pp. 1722–1734, Dec. 1988.

[2] F. X. Canning, "The impedance matrix localization (IML) method for moment-method calculations," *IEEE Antennas Propagat. Soc. Mag.*, vol. 32, no. 5, pp. 18–30, Oct. 1990.

[3] ——, "Transformations that produce a sparse moment method matrix," *J. Electromagnetic Waves Appl.*, vol. 4, no. 9, pp. 893–913, 1990.

[4] ——, "Sparse approximation for solving integral equations with oscillatory kernels," *SIAM J. Sci. Stat. Comput.*, vol. 13, no. 1, pp. 71–87, Jan. 1992.

[5] ——, "Improved impedance matrix localization method," *IEEE Trans. Antenas Propagat.*, vol. 41, no. 5, pp. 659–667, May 1993.

[6] S. Eisler and Y. Leviatan, "Analysis of electromagnetic scattering from metallic and penetrable cylinders with edges using a multifilament current model," *IEE Proc. Pt. H*, vol. 136, no. 6, pp. 431–438, Dec. 1989.

[7] Y. Leviatan, "Analytic continuation considerations when using generalized formulations for scattering problems," *IEEE Trans. Antennas Propagat.*, vol. 38, no. 8, pp. 1259–1263, Aug. 1990.

[8] F. X. Canning, "A new combined field integral equation for impedance matrix localization (IML)," in *IEEE AP-S Int. Symp. Dig.*, 1993, pp. 1140–1143.

[9] P. Regli, personal communication, 1994.

[10] A. Ludwig, "A new technique for numerical electromagnetics," *IEEE Antennas Propagat. Soc. Mag.*, vol. 31, no. 1, pp. 40–41, Feb. 1989.

[11] C. Hafner, *The Generalized Multipole Technique for Computational Electromagnetics.* Norwood, MA: Artech, 1990.

[12] E. Erez and Y. Leviatan, "Current-model analysis of electromagnetic scattering from objects containing a variety of length-scales," *J. Optical Soc. Amer. A*, vol. 11, no. 4, pp. 1500–1504, Apr. 1994.

[13] A. Boag and R. Mittra, "Complex multipole beam approach to 3D electromagnetic scattering problems," *J. Optical Soc. America A*, vol. 11, no. 4, pp. 1505–1512, Apr. 1994.

Yehuda Leviatan (S'82–M'86–SM'88) for a photograph and biography, see p. 933 of the July 1993 issue of this TRANSACTIONS.

Zachi Baharav (S'95) received the B.Sc. degree from Tel-Aviv University and the M.Sc. degree from the Technion-Israel Institute of Technology, both in electrical engineering in 1986 and 1994, respectively. He is currently pursuing the Ph.D. degree in electrical engineering at the Technion.

His research interests include numerical methods in electromagnetics and in fractal image compression.

Ehud Heyman (S'80–M'84–SM'88) for a photograph and biography, see p. 789 of the June 1994 issue of this TRANSACTIONS.